

# Magnetic skyrmion transistor operated with microwaves

Jing Xia,<sup>1</sup> Yangqi Huang,<sup>2,3</sup> Xichao Zhang,<sup>1</sup> Wang Kang,<sup>2,3</sup> Weiwei Wang,<sup>4</sup>  
Chentian Zheng,<sup>2,3</sup> Xiaoxi Liu,<sup>5</sup> Weisheng Zhao,<sup>2,3,\*</sup> and Yan Zhou<sup>1,†</sup>

<sup>1</sup>*School of Science and Engineering, The Chinese  
University of Hong Kong, Shenzhen 518172, China*

<sup>2</sup>*School of Electronic and Information Engineering,  
Beihang University, Beijing 100191, China*

<sup>3</sup>*Fert Beijing Institute, Beihang University, Beijing, China*

<sup>4</sup>*Department of Physics, Ningbo University, Ningbo 315211, China*

<sup>5</sup>*Department of Information Engineering, Shinshu University,  
Wakasato 4-17-1, Nagano 380-8553, Japan*

(Dated: August 23, 2016)

## Abstract

Magnetic skyrmion is a topologically protected magnetic domain-wall structure at nanoscale, which might be a basic building block for advanced spintronic devices. Here, we propose the microwave-driven motion of a magnetic skyrmion in a voltage-gated nanotrack, where the transistor-like function of the magnetic skyrmion is investigated by micromagnetic calculation. It is demonstrated that the microwave field can lead to the motion of the magnetic skyrmion by exciting propagating spin waves, and the motion of the magnetic skyrmion is governed by a gate voltage. We also investigate the microwave-assisted nucleation of a magnetic skyrmion to facilitate the operation of the magnetic skyrmion transistor on the source terminal. It shows that the microwave current with an appropriate frequency can significantly reduce the threshold current density required for the nucleation of the magnetic skyrmion. The proposed magnetic skyrmion transistor operated with the microwave field and current will be useful in future skyrmion-based spintronic circuits.

PACS numbers: 75.78.Fg, 75.78.Cd, 85.70.-w, 85.75.-d

---

\* E-mail: [weisheng.zhao@buaa.edu.cn](mailto:weisheng.zhao@buaa.edu.cn)

† E-mail: [zhouyan@cuhk.edu.cn](mailto:zhouyan@cuhk.edu.cn)

The magnetic skyrmion is an exotic magnetic texture which has a nanoscale vortex-like magnetization structure that is protected by topological invariance [1–3]. In the recent years, the magnetic skyrmion has been experimentally observed in magnetic materials [4–15], semiconductors [16], multiferroic [17] and ferroelectric [18] materials, which indicates that there are diverse potential applications of magnetic skyrmions in the field of spintronics. Indeed, the magnetic skyrmion as information carrier attracts increasing interest for developing the next-generation data storage devices due to its remarkable stability, extremely small size, and low-current depinning property [19–28]. Concurrently, many other applications of the magnetic skyrmions have been proposed and demonstrated, such as skyrmion-based logic devices [29], oscillators [30, 31], and electronic devices [32, 33].

For the practical applications of the magnetic skyrmion, it is required to generate and control the isolated magnetic skyrmion in a feasible way. The magnetic skyrmion can be generated with some kinds of energy injection, such as by applying a spin-polarized current [14, 20], a local heating [34], and a laser [35]. The magnetic skyrmion can also be nucleated with the nanopatterning [36] and be converted from a domain-wall pair [23]. For the manipulation of the magnetic skyrmion, one can use the spin current [19, 21], the spin wave [37–40], as well as the thermal gradient [41–43] to drive the magnetic skyrmion.

Recently, the magnetic skyrmion transistor has been proposed and studied in Refs. [32, 33], in which the magnetic skyrmion is driven by spin current in a voltage-gated nanotrack. In this paper, we study the magnetic skyrmion transistor operated with microwaves, that is, the microwave-field-driven motion and microwave-current-assisted nucleation of the magnetic skyrmion in a voltage-gated nanotrack, where the perpendicular magnetic anisotropy (PMA) of the gate region is controlled by the applied voltage. The microwave field excites the propagating spin waves that drives the motion of the magnetic skyrmion from the source region to the drain region. The magnetic skyrmion at the source region is generated by applying a spin-polarized current with an additional microwave current. Our study shows that the motion of the magnetic skyrmion, which is governed by the gate voltage, can also be controlled by the frequency and amplitude of the microwave field exciting the propagating spin wave. Meanwhile, it shows that the microwave current with a certain frequency can significantly reduce the critical current density required for the nucleation of the magnetic skyrmion. The results indicate that the proposed microwave-field-driven and microwave-current-assisted methods are the effective approaches for building the skyrmion-based transistor. The magnetic skyrmion transistor operated and controlled by the microwave field and current will

be beneficial for the future skyrmion-based spintronic circuits.

## Results

**Magnetic skyrmion transistor driven by a microwave field.** First, we study the magnetic skyrmion transistor driven by a microwave field under the framework of micromagnetics (see Methods for the modeling details). As shown in Fig. 1, the magnetic skyrmion transistor is basically constructed by a nanotrack with the size of  $600 \text{ nm} \times 60 \text{ nm} \times 1 \text{ nm}$ , which has a PMA value of  $K_u = 0.8 \text{ MJ m}^{-3}$  and a Dzyaloshinskii-Moriya interaction (DMI) constant of  $D = 3.5 \text{ mJ m}^{-2}$ . The magnetic nanotrack is sandwiched between the voltage gate electrode and the heavy-metal substrate, where the a voltage-gated region is between  $x = 200 \text{ nm}$  and  $x = 400 \text{ nm}$ . The PMA value within the voltage-gated region  $K_{uv}$  can be adjusted by applying an electric field  $E_{\text{gate}}$  based on the relationship of  $K_{uv} = K_u + \Delta K_{uv} E_{\text{gate}}$  [44–46], where the transition regions between  $K_u$  and  $K_{uv}$  span  $10 \text{ nm}$ . The regions in the nanotrack at the left and right sides of the voltage-gated region are referred to as the source and drain sides, respectively. A microwave antenna is deployed at the left end of the nanotrack ( $0 \text{ nm} < x < 15 \text{ nm}$ ), which can generate a sinusoidal microwave magnetic field  $B_0 \sin(2\pi ft)$  along the  $y$ -direction, where  $B_0$  is the microwave amplitude and  $f$  is the microwave frequency. The magnetic nanotrack is almost magnetized along  $+z$ -direction in our setup. A magnetic skyrmion is created and relaxed at the source side of the nanotrack ( $x = 100 \text{ nm}$ ) by a skyrmion injector which can be fabricated by placing a magnetic tunnel junction (MTJ) upon the source side of the nanotrack [26].

Figure 1 illustrates the initial, ON and OFF states of the magnetic skyrmion transistor. At the initial state, both the microwave antenna and the voltage gate are turned off, the magnetic skyrmion remains in its position on the source side at  $x = 100 \text{ nm}$ . At the ON state, the antenna is turned on ( $B_0 = 500 \text{ mT}$ ,  $f = 75 \text{ GHz}$ ) but the voltage gate is turned off. The microwave field pulse applied at the left end of the nanotrack excites spin waves propagating toward the drain side of the nanotrack, driving the magnetic skyrmion into motion. The moving skyrmion passes the voltage-gated region and reaches the drain side of the nanotrack at  $t = 9 \text{ ns}$ , which can be detected by the skyrmion reader at the drain side [26]. At the OFF state, both the microwave antenna and the voltage gate are turned on. The spin waves excited by the microwave field drive the magnetic skyrmion moving towards the right. On the other hand, the gate voltage, which results in the change of the PMA value  $K_{uv}$  in the voltage-gated region, leads to the stop of skyrmion when it approaches the gate-induced potential barrier. As shown in Fig. 1, when the PMA value in the

voltage-gated region is larger than that of the intrinsic value, i.e.  $K_{uv} = 1.025K_u$ , the skyrmion stops at the potential barrier at the boundary between the source side and the voltage-gated region. When the PMA value in the voltage-gated region is smaller than that of the intrinsic value, i.e.  $K_{uv} = 0.975K_u$ , the skyrmion stops at the potential barrier at the boundary between the voltage-gated region and the drain side. For both OFF states, the skyrmion reaches the equilibrium state within  $t = 30$  ns under the driving force from the microwave-induced spin waves and the repulsive force from the potential barrier.

Figure 2 shows the trajectories of the skyrmion motion in the magnetic skyrmion transistor driven by the microwave-induced spin waves at the ON and OFF states with different amplitudes ( $B_0 = 500$  mT or 650 mT,  $f = 75$  GHz). As shown in Fig. 2a, the magnetic skyrmion transistor is in the ON state, where the microwave antenna is turned on and the voltage gate is turned off. The PMA value in the voltage-gated region equals that of the intrinsic value, i.e.  $K_{uv} = K_u$ . The skyrmion moves from the source side to the drain side within 10 ns. It is worth mentioning that the transverse motion of the skyrmion in the  $y$ -direction is caused by the skyrmion Hall effect [24]. Due to the decay of the microwave-induced spin waves and the repulsion from the edge at the right end of the nanotrack, the magnetic skyrmion is finally relaxed at the drain side at  $t = 30$  ns. When the magnetic skyrmion transistor is in the OFF state, as shown in Fig. 2b, where the microwave antenna and the voltage are turned on, the PMA value in the voltage-gated is larger than that of the intrinsic value, i.e.  $K_{uv} = 1.025K_u$ . The magnetic skyrmion driven by the microwave-induced spin waves moves toward the drain side. However, the magnetic skyrmion cannot surmount the potential barrier at the boundary between the source side with lower PMA and the voltage-gated region with higher PMA. It can be seen that the center of the magnetic skyrmion can enter the voltage-gated region for a short time driven by the strong excited spin wave emitted from the microwave antenna. Nevertheless, the magnetic skyrmion is repelled by the potential barrier. The combined effects of the driving force supplied from the microwave antenna, the repulsive force provided by the voltage gate and the Magnus force exerted on the magnetic skyrmion lead to the motion of the magnetic skyrmion in a spiral trajectory. The skyrmion eventually reaches equilibrium and stops near the boundary between the source side and the voltage-gated region. Figure 2c shows the other OFF state, where the microwave antenna and the voltage are turned on, the PMA value in the voltage-gated is smaller than that of the intrinsic value, i.e.  $K_{uv} = 0.975K_u$ . The magnetic skyrmion driven by the microwave-induced spin waves moves toward the drain side. In contrast to the OFF state shown in Fig. 2b, the magnetic skyrmion passes the boundary between

the source side with higher PMA and the voltage-gated region with lower PMA, where a potential well is induced. However, the magnetic skyrmion cannot penetrate the potential barrier at the boundary between the voltage-gated region with lower PMA and the drain side with higher PMA. Similar to the OFF state shown in Fig. 2b, the magnetic skyrmion shows a spiral trajectory of motion, and finally stops near the boundary between the voltage-gated region and the drain side. In three cases, the frequency of the microwave is fixed at  $f = 75$  GHz, while two amplitudes of  $B_0 = 500$  mT and  $B_0 = 650$  mT are applied, respectively. It can be seen that the transverse shift of the skyrmion in the  $y$ -direction increases with the amplitude of the microwave. Indeed, the speed of the skyrmion increases with the amplitude of the microwave.

Figure 3 shows the trajectories of the skyrmion in the magnetic skyrmion transistor at the ON and OFF states driven by the microwave-induced spin waves with different frequencies ( $B_0 = 500$  mT,  $f = 75$  GHz or 78 GHz). Figure 3a shows the ON state, where the microwave antenna is turned on and the voltage gate is turned off. The PMA value in the voltage-gated region equals that of the intrinsic value, i.e.  $K_{uv} = K_u$ . Figure 3b shows the OFF state, where the microwave antenna and the voltage are turned on, the PMA value in the voltage-gated is larger than that of the intrinsic value, i.e.  $K_{uv} = 1.025K_u$  or  $1.050K_u$ . Figure 3c shows the other OFF state, where the microwave antenna and the voltage are turned on, the PMA value in the voltage-gated is smaller than that of the intrinsic value, i.e.  $K_{uv} = 0.975K_u$ . In three cases, the amplitude of the microwave is fixed at  $B_0 = 500$  mT, while two frequencies of  $f = 75$  GHz and  $f = 78$  GHz are applied, respectively. It should be noted that in Fig. 3c, we set  $K_{uv} = 1.025K_u$  for the case of  $f = 75$  GHz, while  $K_{uv} = 1.050K_u$  for the case of  $f = 78$  GHz, in order to ensure the OFF state. It can be seen that the transverse shift of the skyrmion in the  $y$ -direction increases with the frequency of the microwave. Indeed, the speed of the skyrmion increases with the frequency of the microwave.

Figure 4 shows the working windows of the magnetic skyrmion transistor driven and controlled by the microwave antenna and the voltage gate. As shown in Fig. 4a, the excitation field amplitude of the microwave antenna is fixed at  $B_0 = 500$  mT, while the excitation field frequency of the microwave antenna is varied in the range between  $f = 72$  GHz and  $f = 78$  GHz. Obviously, when the voltage gate is turned off, i.e.  $K_{uv} = K_u$ , the magnetic skyrmion transistor is always in the ON state, where the magnetic skyrmion moves from the source side to the drain side in a certain time. When the voltage gate is turned on, which adjusts the  $K_{uv}$  to be in the range of  $0.995K_u$  and  $1.015K_u$ , the magnetic skyrmion transistor is still in the ON state, as the gate-induced potential barrier is not strong enough to stop the magnetic skyrmion from passing through. When the  $K_{uv}$

is further increased to be larger than  $1.02K_u$  or decreased to be smaller than  $0.99K_u$ , the working state of the magnetic skyrmion transistor switches to the OFF state at  $f = 72$  GHz. However, it can be seen that when  $f$  increases to 78 GHz, the magnetic skyrmion under stronger driving force provided by the microwave antenna can overcome the potential barrier induced by the voltage gate in the range of  $K_{uv} = 0.99K_u$  and  $K_{uv} = 1.03K_u$ . Because the potential barrier at the boundary between the source side with lower PMA and the voltage-gated region with higher PMA is closer to the antenna than the one at the boundary between the voltage-gated region with lower PMA and the drain side with higher PMA, the skyrmion experiences stronger driving force when it is approaching the former potential barrier. Thus, the potential barrier at the boundary between the source side with lower PMA and the voltage-gated region with higher PMA is easier to be penetrated by the magnetic skyrmion at the same  $B_0$  and  $f$ . Similar results are shown in Fig. 4b, where the excitation field frequency of the microwave antenna is fixed at  $f = 75$  GHz, while the excitation field amplitude of the microwave antenna is varied in the range between  $B_0 = 350$  mT and  $B_0 = 650$  mT.

Figure 5 shows the working windows of the magnetic skyrmion transistor at different DMI constants and microwave antenna parameters with a fixed voltage gate-induced PMA value  $K_{uv}$ . Figure 5a,b show the working state of the magnetic skyrmion transistor at  $K_{uv} = 1.020K_u$  as functions of the DMI constant  $D$  and antenna frequency  $f$ , and as functions of DMI constant  $D$  and antenna amplitude  $B_0$ , respectively. Figure 5c,d show the working state of the magnetic skyrmion transistor at  $K_{uv} = 0.995K_u$  as functions of the DMI constant  $D$  and antenna frequency  $f$ , and as functions of DMI constant  $D$  and antenna amplitude  $B_0$ , respectively. It can be seen that the magnetic skyrmion in a nanotrack with a smaller DMI constant  $D$  is easier to overcome the potential barrier at given  $K_{uv}$ ,  $B_0$  and  $f$ .

**Nucleation of the magnetic skyrmion assisted by a microwave current.** With respect to the generation of the magnetic skyrmion at the source terminal of the magnetic skyrmion transistor, we also implement the microwave-current-assisted nucleation of the magnetic skyrmion. For the sake of low computational complexity, here we consider the model of a nanodisk instead of the nanotrack studied in last section. As shown in Fig. 6a, a magnetic nanodisk initially magnetized along  $+z$ -direction is built in the simulation, which has a diameter of 80 nm and a thickness of 1 nm. The current injection nano-contact is of 24 nm in diameter and set in the central region of the nanodisk.

In order to create the magnetic skyrmion in the nanodisk, we utilize a microwave-assisted vertical spin-polarized current, which can be expressed as  $j_{\text{total}} = j_0 \sin 2\pi f_{\text{AC}} t + j_{\text{DC}}$ . Here,  $j_0$  is the amplitude of the microwave current,  $f_{\text{AC}}$  is the frequency of the microwave current, and  $j_{\text{DC}}$  is the current density of the DC current. We focus on the threshold current density  $j_{\text{th}}$  which is defined as the minimal  $j_{\text{DC}}$  required to nucleate the magnetic skyrmion within a 2 ns injection of spin current and microwave current. The applied current duration is fixed to 2 ns in this work.

Figure 6 shows the nucleation process of the magnetic skyrmion in the presence and absence of the microwave current. As shown in Fig. 6a, the DC current density  $j_{\text{DC}}$  is fixed at  $j_{\text{DC}} = 1.8 \times 10^{12} \text{ A m}^{-2}$ , and the frequency of the microwave current is set as  $f_{\text{AC}} = 53 \text{ GHz}$ . In order to indicate the nucleation of the magnetic skyrmion, we calculate and show  $m_x, m_y, m_z$ , and the skyrmion number  $Q$  as functions of time. The nucleation current is injected at  $t = 0 \text{ ns}$ . Then the skyrmion number  $Q$  starts to fluctuate while the magnetization stays quasi-uniform with a spin wave transferring from the center to the edge, indicating the injection of energy. At  $t = 0.39 \text{ ns}$ , the magnetization of the central region reverses in a very short time ( $\sim 0.01 \text{ ns}$ ), and generates a stable magnetic skyrmion, resulting in a rapid jump of the skyrmion number from  $Q \sim -0.1$  to  $Q \sim 1$ . After this rapid change, the skyrmion number stabilizes at  $Q \sim 1$ , marking a success of the skyrmion nucleation. It should be noted that we also find the breathing of the magnetic skyrmion after its nucleation, which can be seen from the snapshots and the fluctuation of  $m_z$  during the period of  $t = 0.39 \sim 0.60 \text{ ns}$ . At  $t = 0.60 \text{ ns}$ , the magnetic skyrmion stops breathing and becomes a stable magnetic skyrmion. Figure 6b shows the case in the absence of the assistance of the microwave current. With the identical DC current density, no magnetic skyrmion is formed in the nanodisk in the absence of the microwave current. We also calculate the skyrmion number  $Q$  and find a slight fluctuation during the time within which the DC current is applied. The skyrmion number is equal to  $Q \sim 0$  during the simulation. We also calculate the skyrmion number  $Q$  and only find a slight fluctuation near 0 during the time within which the DC current is applied. It indicates that the DC current density of  $1.8 \times 10^{12} \text{ A m}^{-2}$  is smaller than the threshold current.

Figure 7 shows the threshold current density  $j_{\text{th}}$  as functions of frequency  $f_{\text{AC}}$  of the microwave current with a fixed microwave amplitude  $j_0 = 1.3 \times 10^{12} \text{ A m}^{-2}$ . Since the power is in direct proportional to  $j_{\text{total}}^2$ , where  $j_{\text{total}} = j_0 \sin 2\pi f_{\text{AC}} t + j_{\text{th}}$ , we can obtain that the power is in direct proportional to  $j_{\text{th}}^2 + j_0^2/2$ . Both the threshold current density and the corresponding  $j_{\text{th}}^2 + j_0^2/2$  have been shown in Fig. 7. As can be seen, the average  $j_{\text{th}}$  equals  $1.8 \times 10^{12} \text{ A m}^{-2}$  approximately when the microwave current is injected. There is an obvious frequency range,  $50 \text{ GHz} \sim 56 \text{ GHz}$ , where



the required current density is much less than the average one. As a result, the energy consumption in whole process is also reduced as the injection time is fixed to be 2 ns. It means that the energy consumption can be reduced with modulating the frequency of the additional microwave current. This behavior can be explained with the resonance below.

Figure 8 shows normalized power spectral densities and the threshold current density  $j_{\text{th}}$  as a function of the microwave current frequency  $f_{\text{AC}}$  with a fixed amplitude of  $j_0 = 1.0 \times 10^{12} \text{ A m}^{-2}$ . And the step size of the microwave current frequency is adopted as 0.2 GHz. In order to obtain the power spectral density, the equilibrium magnetization configuration  $\mathbf{m}(0)$  has been calculated firstly. Then a sinc-function field  $H_0 \sin(2\pi f_H t)/(2\pi f_H t)$  with  $H_0 = 0.5 \text{ mT}$  and  $f_H = 100 \text{ GHz}$  is applied along  $x$ -axis. We record the time-dependent magnetization configuration  $\mathbf{m}(t)$  every  $\Delta t = 5 \text{ ps}$  and analyze  $\Delta m_x(t)$  with spatially averaged and spatially resolved methods [47, 48], as shown in Fig. 8b. Similarly, the power spectral densities of  $\Delta m_y$  and  $\Delta m_z$  are obtained with the sinc-function field applied along  $y$ -axis and  $z$ -axis, as shown in Fig. 8c,d, respectively. Resonances have been detected at 44 GHz, 49 GHz, 58 GHz, 61 GHz, 62 GHz, 64 GHz, 66 GHz, and 69 GHz, labeled by number from 1 to 8.  $j_{\text{th}}$  decreases when the frequency is in the vicinity the resonance frequency, which can be seen obviously from the case of resonance peaks 1 and 5. Resonance peaks 2, 3, 6, 7, and 8 lead fluctuations in the threshold current. When the frequency of the microwave current matches the resonance frequency, the momenta of the spin current are resonantly transferred to the local magnetic moment, resulting in the decrease of the total energy consumption.

Besides, we also have investigated the effect of the amplitude of the microwave current on the threshold current density, as shown in Fig. 9. In this case, the frequency is fixed,  $f_{\text{AC}} = 53 \text{ GHz}$ , and the step size of the amplitude of the microwave current is  $0.02 \times 10^{12} \text{ A m}^{-2}$ . Both the threshold current density and the corresponding  $j_{\text{th}}^2 + j_0^2/2$  have been shown in Fig. 9. If there is no microwave current injected,  $j_0 = 0$ , the DC current required to create skyrmion within 2 ns reaches  $1.8 \times 10^{12} \text{ A m}^{-2}$  in the given sample disk, which drops to  $1.4 \times 10^{12} \text{ A m}^{-2}$  when an additional microwave current with  $j_0 = 1.6 \times 10^{12} \text{ A m}^{-2}$  is superimposed on the DC. The injection of microwave current also impacts the value of  $j_{\text{th}}^2 + j_0^2/2$  which is direct proportional to the power as well as the energy consumption with fixed injection time. The results show that the amplitude and frequency of the assisted microwave current facilitate the creation of magnetic skyrmions. As a result, the energy consumption in the whole process is reduced as the injection time is fixed. So, the energy consumption required to create skyrmions in a limited time can be



reduced by applying a microwave current with particular amplitude and frequency.

## Discussion

We have proposed a magnetic skyrmion transistor operated and controlled by microwaves. It is demonstrated that the microwave field can lead to the motion of the magnetic skyrmion by exciting propagating spin waves, where the motion of the magnetic skyrmion is governed by a gate voltage. Besides, the creation of the magnetic skyrmion at the source region of the magnetic skyrmion transistor is also assisted by a microwave current. It shows that the microwave current can reduce the energy consumption required for the nucleation of the magnetic skyrmion with a fixed time, and the reduction is significant when its frequency is close to the resonance frequency. Our results on the magnetic skyrmion transistor operated and controlled by the microwave field and microwave current might be useful in the design of future skyrmion-based spintronic circuits.

## Methods

**Model and simulation details.** The three-dimensional (3D) micromagnetic simulation is performed by using the 1.2a5 release of the Object Oriented MicroMagnetic Framework (OOMMF) software developed at the National Institute of Standards and Technology (NIST) [49]. The simulation is handled by the OOMMF extensible solver (OXS) objects of the standard OOMMF distribution with the OXS extension module for including the interface-induced Dzyaloshinskii-Moriya interaction (DMI), that is, the `Oxs_DMExchange6Ngbr` class [50–53].

The interfacial DMI in the ultra-thin magnetic film with perpendicular magnetic anisotropy (PMA) placed on the heavy-metal substrate with high spin-orbit coupling is expressed as [51]

$$E_{\text{DM}} = \sum_{\langle i,j \rangle} d_{\text{DM}}(\mathbf{u}_{ij} \times \hat{\mathbf{z}}) \cdot (\mathbf{S}_i \times \mathbf{S}_j), \quad (1)$$

with  $d_{\text{DM}}$  the DMI coupling energy,  $\mathbf{u}_{ij}$  the unit vector between spins  $\mathbf{S}_i$  and  $\mathbf{S}_j$ , and  $\hat{\mathbf{z}}$  the normal to the interface, oriented from the heavy-metal substrate to the magnetic layer. In the continuous micromagnetic model, the DMI reads

$$E_{\text{DM}} = b \int D \left[ \left( m_x \frac{\partial m_z}{\partial x} - m_z \frac{\partial m_x}{\partial x} \right) + \left( m_y \frac{\partial m_z}{\partial y} - m_z \frac{\partial m_y}{\partial y} \right) \right] d^2 \mathbf{r}, \quad (2)$$

with  $D$  the continuous DMI constant,  $b$  the magnetic sample thickness.  $m_x$ ,  $m_y$  and  $m_z$  are the components of the reduced magnetization  $\mathbf{m}$ , where  $\mathbf{m} = \mathbf{M}/M_S$ . The link between  $D$  and  $d_{\text{DM}}$  is  $d_{\text{DM}}/ab$  for a (001) interface and  $d_{\text{DM}}\sqrt{3}/ab$  for a (111) interface with  $a$  the atomic distance [50], of which the latter case is employed in this paper.

The 3D time-dependent magnetization dynamics in the simulation is controlled by the Landau-Lifshitz-Gilbert (LLG) equation including the spin-transfer torque (STT) term [49, 54]. Specifically, when no spin-polarized current is injected into the simulated system, that is, the STT term is deactivated, the LLG equation reads

$$\frac{d\mathbf{M}}{dt} = -\gamma_0 \mathbf{M} \times \mathbf{H}_{\text{eff}} + \frac{\alpha}{M_S} (\mathbf{M} \times \frac{d\mathbf{M}}{dt}), \quad (3)$$

where  $\mathbf{M}$  is the magnetization,  $\mathbf{H}_{\text{eff}}$  is the effective field,  $t$  is the time,  $\alpha$  is the Gilbert damping coefficient, and  $\gamma_0$  is the gyromagnetic ratio. The effective field  $\mathbf{H}_{\text{eff}}$  is expressed as follows

$$\mathbf{H}_{\text{eff}} = -\mu_0^{-1} \frac{\delta \varepsilon}{\delta \mathbf{M}}. \quad (4)$$

The average energy density  $\varepsilon$  is a function of  $\mathbf{M}$  specified by

$$\begin{aligned} \varepsilon = A[\nabla(\frac{\mathbf{M}}{M_S})]^2 - K \frac{(\mathbf{n} \cdot \mathbf{M})^2}{M_S^2} - \mu_0 \mathbf{M} \cdot \mathbf{H} \\ - \frac{\mu_0}{2} \mathbf{M} \cdot \mathbf{H}_d(\mathbf{M}) + \varepsilon_{\text{DM}}, \end{aligned} \quad (5)$$

where  $A$  and  $K$  are the exchange and anisotropy energy constants, respectively.  $\mathbf{H}$  and  $\mathbf{H}_d(\mathbf{M})$  are the applied and magneto-static self-interaction fields while  $M_S = |\mathbf{M}(r)|$  is the saturation magnetization.  $\varepsilon_{\text{DM}}$  is the energy density of the DMI, which has the form

$$\varepsilon_{\text{DM}} = \frac{D}{M_S^2} (M_z \frac{\partial M_x}{\partial x} + M_z \frac{\partial M_y}{\partial y} - M_x \frac{\partial M_z}{\partial x} - M_y \frac{\partial M_z}{\partial y}), \quad (6)$$

where the  $M_x$ ,  $M_y$  and  $M_z$  are the components of the magnetization  $\mathbf{M}$ . The five terms at the right side of equation (5) correspond to the exchange energy, the anisotropy energy, the applied field (Zeeman) energy, the magneto-static (demagnetization) energy and the DMI energy, respectively. For the simulated system, the spin-polarized current with the injection of current-perpendicular-to-the-plane (CPP) geometry is considered. The in-plane spin transfer torque is written as [20]

$$\tau_{\text{in-plane}} = -\frac{u}{b} \mathbf{m} \times (\mathbf{m} \times \mathbf{p}), \quad (7)$$

where  $u = \frac{\gamma_0 \hbar j P}{2\mu_0 e M_S}$ ,  $j$  is the current density,  $P$  is the spin polarization,  $\mathbf{p} = -\hat{z}$  is the unit electron polarization direction,  $b$  is the thickness of the ferromagnetic layer. Thus, the LLG equation (3) of

magnetization motion augmented with STT terms reads

$$\frac{d\mathbf{m}}{dt} = -\gamma_0 \mathbf{m} \times \mathbf{h}_{\text{eff}} + \alpha \left( \mathbf{m} \times \frac{d\mathbf{m}}{dt} \right) - \frac{\gamma_0 \hbar j P}{2\mu_0 e b M_S} [\mathbf{m} \times (\mathbf{m} \times \mathbf{p})], \quad (8)$$

where  $\mathbf{h}_{\text{eff}}$  is the reduced effective field, that is,  $\mathbf{h}_{\text{eff}} = \mathbf{H}_{\text{eff}}/M_S$ . The models built in the micromagnetic simulation are divided into regular cells with the constant size of  $2 \text{ nm} \times 2 \text{ nm} \times 1 \text{ nm}$ , which allows for a trade-off between numerical accuracy and computational efficiency. The Oersted field is neglected in the simulation for simplicity due to its minor contribution to the effect field.

For micromagnetic simulations, the parameters of the magnetic layer are adopted from Refs. [19, 20, 22]: Gilbert damping coefficient  $\alpha = 0.02$ ; gyromagnetic ratio  $\gamma = -2.211 \times 10^5 \text{ m A}^{-1} \text{ s}^{-1}$ ; saturation magnetization  $M_S = 580 \text{ kA m}^{-1}$ ; intralayer exchange stiffness  $A = 15 \text{ pJ m}^{-1}$ ; DMI constant  $D = 0 \sim 4 \text{ mJ m}^{-2}$ ; PMA  $K_u = 0.8 \text{ MJ m}^{-3}$ ; and spin polarization rate  $P = 0.4$  unless otherwise specified.

The stable magnetic skyrmion stabilized by the interface-induced DMI is the hedgehog-like skyrmion, which has a radial in-plane magnetization profile. It is characterized by the Pontryagin number  $Q$  [23, 29], namely the topological charge in the planar system, which is defined by

$$Q = \int dx dy \rho_{\text{sky}}(x), \quad (9)$$

where the  $\rho_{\text{sky}}$  reads

$$\rho_{\text{sky}}(x) = -\frac{1}{4\pi} \mathbf{m}(x) \cdot (\partial_x \mathbf{m}(x) \times \partial_y \mathbf{m}(x)). \quad (10)$$

The number  $Q$  is referred to as the skyrmion number. When the background magnetization and the skyrmion core are pointing in the  $+z$ -direction and the  $-z$ -direction, respectively, the skyrmion number  $Q$  equals  $+1$ . Otherwise, when the background magnetization and the skyrmion core are pointing in the  $-z$ -direction and the  $+z$ -direction, respectively, the skyrmion number  $Q$  equals  $-1$ . In this paper, as we are assuming that the background magnetization is aligned along the  $+z$ -direction at the initial state, thus the skyrmion number of the relaxed (stable/metastable) skyrmion equals one,  $Q = +1$ .

---

[1] Roszler, U. K., Bogdanov, A. N. & Pfleiderer, C. Spontaneous skyrmion ground states in magnetic metals. *Nature* **442**, 797-801 (2006).

- [2] Nagaosa, N. & Tokura, Y. Topological properties and dynamics of magnetic skyrmions. *Nat. Nano.* **8**, 899-911 (2013).
- [3] von Bergmann, K., Kubetzka, A., Pietzsch, O. & Wiesendanger, R. Interface-induced chiral domain walls, spin spirals and skyrmions revealed by spin-polarized scanning tunneling microscopy. *J. Phys.: Condens. Matter* **26**, 394002 (2014).
- [4] Mühlbauer, S. *et al.* Skyrmion lattice in a chiral magnet. *Science* **323**, 915-919 (2009).
- [5] Yu, X. Z. *et al.* Real-space observation of a two-dimensional skyrmion crystal. *Nature* **465**, 901-904 (2010).
- [6] Heinze, S. *et al.* Spontaneous atomic-scale magnetic skyrmion lattice in two dimensions. *Nat. Phys.* **7**, 713-718 (2011).
- [7] Yu, X. Z. *et al.* Near room-temperature formation of a skyrmion crystal in thin-films of the helimagnet FeGe. *Nat. Mater.* **10**, 106-109 (2011).
- [8] Schulz, T. *et al.* Emergent electrodynamics of skyrmions in a chiral magnet. *Nat. Phys.* **8**, 301-304 (2012).
- [9] Romming, N. *et al.* Writing and deleting single magnetic skyrmions. *Science* **341**, 636-639 (2013).
- [10] Oike, H. *et al.* Interplay between topological and thermodynamic stability in a metastable magnetic skyrmion lattice. *Nat. Phys.* **12**, 62-66 (2016).
- [11] Du, H. *et al.* Edge-mediated skyrmion chain and its collective dynamics in a confined geometry. *Nat. Commun.* **6**, 8504 (2015).
- [12] Nii, Y. *et al.* Uniaxial stress control of skyrmion phase. *Nat. commun.* **6**, 8539 (2015).
- [13] Buttner, F. *et al.* Dynamics and inertia of skyrmionic spin structures. *Nat. Phys.* **11**, 225-228 (2015).
- [14] Jiang, W. *et al.* Blowing magnetic skyrmion bubbles. *Science* **349**, 283-286 (2015).
- [15] Woo, S. *et al.* Observation of room-temperature magnetic skyrmions and their current-driven dynamics in ultrathin metallic ferromagnets. *Nat. Mater.* **15**, 501-506 (2016).
- [16] Kezsmarki, I. *et al.* Neel-type skyrmion lattice with confined orientation in the polar magnetic semiconductor GaV4S8. *Nat. Mater.* **14**, 1116-1122 (2015).
- [17] Seki, S., Yu, X. Z., Ishiwata, S. & Tokura, Y. Observation of skyrmions in a multiferroic material. *Science* **336**, 198-201 (2012).
- [18] Nahas, Y. *et al.* Discovery of stable skyrmionic state in ferroelectric nanocomposites. *Nat. Commun.* **6**, 8542 (2015).
- [19] Fert, A., Cros, V. & Sampaio, J. Skyrmions on the track. *Nat. Nano.* **8**, 152-156 (2013).

- [20] Sampaio, J., Cros, V., Rohart, S., Thiaville, A. & Fert, A. Nucleation, stability and current-induced motion of isolated magnetic skyrmions in nanostructures. *Nat. Nano.* **8**, 839-844 (2013).
- [21] Iwasaki, J., Mochizuki, M. & Nagaosa, N. Current-induced skyrmion dynamics in constricted geometries. *Nat. Nano.* **8**, 742-747 (2013).
- [22] Tomasello, R. *et al.* A strategy for the design of skyrmion racetrack memories. *Sci. Rep.* **4**, 6784 (2014).
- [23] Zhou, Y. & Ezawa, M. A reversible conversion between a skyrmion and a domain-wall pair in a junction geometry. *Nat. Commun.* **5**, 4652 (2014).
- [24] Zhang, X., Zhou, Y. & Ezawa, M. Magnetic bilayer-skyrmions without skyrmion Hall effect. *Nat. Commun.* **7**, 10293 (2016).
- [25] Zhang, X. *et al.* Skyrmion-skyrmion and skyrmion-edge repulsions in skyrmion-based racetrack memory. *Sci. Rep.* **5**, 7643 (2015).
- [26] Koshibae, W. *et al.* Memory functions of magnetic skyrmions. *Japan. J. Appl. Phys.* **54**, 053001 (2015).
- [27] Dai, Y., Wang, H., Yang, T., Ren, W. & Zhang, Z. Flower-like dynamics of coupled skyrmions with dual resonant modes by a single-frequency microwave magnetic field. *Sci. Rep.* **4**, 6153 (2014).
- [28] Beg, M. *et al.* Ground state search, hysteretic behaviour, and reversal mechanism of skyrmionic textures in confined helimagnetic nanostructures. *Sci. Rep.* **5**, 17137 (2015).
- [29] Zhang, X., Ezawa, M. & Zhou, Y. Magnetic skyrmion logic gates: conversion, duplication and merging of skyrmions. *Sci. Rep.* **5**, 9400 (2015).
- [30] Zhou, Y. *et al.* Dynamically stabilized magnetic skyrmions. *Nat. Commun.* **6**, 8193 (2015).
- [31] Zhang, S. *et al.* Current-induced magnetic skyrmions oscillator. *New J. Phys.* **17**, 023061 (2015).
- [32] Zhang, X., Zhou, Y., Ezawa, M., Zhao, G. P. & Zhao, W. Magnetic skyrmion transistor: skyrmion motion in a voltage-gated nanotrack. *Sci. Rep.* **5**, 11369 (2015).
- [33] Upadhyaya, P., Yu, G., Amiri, P. K. & Wang, K. L. Electric-field guiding of magnetic skyrmions. *Phys. Rev. B* **92**, 134411 (2015).
- [34] Koshibae, W. & Nagaosa, N. Creation of skyrmions and antiskyrmions by local heating. *Nat. Commun.* **5**, 5148 (2013).
- [35] Finazzi, M. *et al.* Laser-induced magnetic nanostructures with tunable topological properties. *Phys. Rev. Lett.* **110**, 177205 (2013).
- [36] Sun, L. *et al.* Creating an artificial two-dimensional skyrmion crystal by nanopatterning. *Phys. Rev.*

- Lett.* **110**, 167201 (2013).
- [37] Komineas, S. & Papanicolaou, N. Skyrmion dynamics in chiral ferromagnets. *Phys. Rev. B* **92**, 064412 (2015).
  - [38] Schütte, C. & Garst, M. Magnon-skyrmion scattering in chiral magnets. *Phys. Rev. B* **90**, 094423 (2014).
  - [39] Zhang, X. *et al.* All-magnetic control of skyrmions in nanowires by a spin wave. *Nanotechnology* **26**, 225701 (2015).
  - [40] Ma, F., Zhou, Y., Braun, H. B. & Lew, W. S. Skyrmion-based dynamic magnonic crystal. *Nano Letters* **15**, 4029-4036 (2015).
  - [41] Everschor, K. *et al.* Rotating skyrmion lattices by spin torques and field or temperature gradients. *Phys. Rev. B* **86**, 054432 (2012).
  - [42] Kong, L. & Zang, J. Dynamics of an insulating skyrmion under a temperature gradient. *Phys. Rev. Lett.* **111**, 067203 (2013).
  - [43] Lin, S.-Z., Batista, C. D., Reichhardt, C. & Saxena, A. AC current generation in chiral magnetic insulators and skyrmion motion induced by the spin Seebeck effect. *Phys. Rev. Lett.* **112**, 187203 (2014).
  - [44] Maruyama, T. *et al.* Large voltage-induced magnetic anisotropy change in a few atomic layers of iron. *Nat. Nano.* **4**, 158-161 (2009).
  - [45] Shiota, Y. *et al.* Quantitative evaluation of voltage-induced magnetic anisotropy change by magnetoresistance measurement. *Appl. Phys. Express* **4**, 043005 (2011).
  - [46] Schellekens, A., van den Brink, A., Franken, J., Swagten, H. & Koopmans, B. Electric-field control of domain wall motion in perpendicularly magnetized materials. *Nat. Commun.* **3**, 847 (2012).
  - [47] Beg, M. *et al.* Dynamics of skyrmionic states in confined helimagnetic nanostructures. *arXiv* 1604.08347, <http://arxiv.org/abs/1604.08347> (2016). (Accessed: 1st May 2016)
  - [48] Baker, A. *et al.* Proposal of a micromagnetic standard problem for ferromagnetic resonance simulations. *arXiv* 1603.05419, <http://arxiv.org/abs/1603.05419> (2016). (Accessed: 20th March 2016)
  - [49] Donahue, M. J. & Porter, D. G. *OOMMF User's Guide, Version 1.0 Interagency Report NISTIR 6376* (National Institute of Standards and Technology, Gaithersburg, MD, 1999).
  - [50] Rohart, S. & Thiaville, A. *OOMMF Oxs extension module of the Dzyaloshinskii-Moriya interaction*. (2012) Available at: [www.lps.u-psud.fr/spip.php?article2252](http://www.lps.u-psud.fr/spip.php?article2252). (Accessed: 1st May 2013)
  - [51] Rohart, S. & Thiaville, A. Skyrmion confinement in ultrathin film nanostructures in the presence of

- Dzyaloshinskii-Moriya interaction. *Phys. Rev. B* **88**, 184422 (2013).
- [52] Dzyaloshinsky, I. A thermodynamic theory of "weak" ferromagnetism of antiferromagnetics. *J. Phys. Chem. Solids* **4**, 241-255 (1958).
- [53] Moriya, T. Anisotropic superexchange interaction and weak ferromagnetism. *Phys. Rev.* **120**, 91-98 (1960).
- [54] Xiao, J., Zangwill, A. & Stiles, M. D. Boltzmann test of Slonczewski's theory of spin-transfer torque. *Phys. Rev. B* **70**, 172405 (2004).



## **Acknowledgements**

Y.Z. acknowledges the support by Shenzhen Fundamental Research Fund under Grant No. JCYJ20160331164412545. W.S.Z. acknowledges the support by the projects from the Chinese Postdoctoral Science Foundation (No. 2015M570024), National Natural Science Foundation of China (Projects No. 61501013, No. 61471015 and No. 61571023), Beijing Municipal Commission of Science and Technology (Grant No. D15110300320000), and the International Collaboration Project (No. 2015DFE12880) from the Ministry of Science and Technology of China. X.Z. was supported by JSPS RONPAKU (Dissertation Ph.D.) Program.

## **Author Contributions**

Y.Z. conceived the main idea. Y.Z., W.S.Z. and X.L. coordinated and supervised the work. J.X., Y.H. and X.Z. performed the numerical simulations. J.X., W.K., W.W. and C.Z. analyzed the data. All authors discussed the results and prepared the manuscript.

## **Additional Information**

Correspondence and requests for materials should be addressed to W.Z. and Y.Z.

## **Competing Financial Interests**

The authors declare no competing financial interests.

## Figure Legends

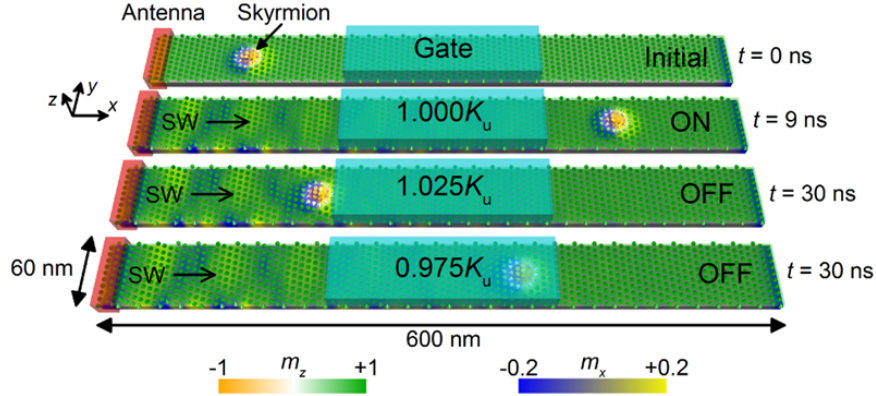


**Figure 1.** The microwave-driven magnetic skyrmion transistor at different working states (initial state, ON state, and OFF state). The length along the  $x$ -axis, width along the  $y$ -axis, and thickness along the  $z$ -axis of the magnetic nanotrack are equal to 600 nm, 60 nm and 1 nm, respectively. The PMA of the nanotrack  $K_u = 0.8 \text{ MJ m}^{-3}$ . The DMI of the nanotrack  $D = 3.5 \text{ mJ m}^{-2}$ . A magnetic skyrmion is first created and relaxed at the left (source) side of the nanotrack ( $x = 100 \text{ nm}$ ). An electrode is placed on the center (gate) of the nanotrack ( $200 \text{ nm} < x < 400 \text{ nm}$ ) for locally changing PMA. An oscillating magnetic field  $B_0 \sin(2\pi ft)$  along the  $y$ -direction is applied at the left end of the nanotrack ( $0 \text{ nm} < x < 15 \text{ nm}$ ) by a microwave antenna (here,  $B_0 = 500 \text{ mT}$ ,  $f = 75 \text{ GHz}$ ). At the initial state, both the microwave antenna and voltage gate are turned off. The magnetic skyrmion keeps its position on the source side. At the ON state, the microwave antenna is turned on but the voltage gate is turned off. The magnetic skyrmion driven by the microwave-excited spin wave (SW) passes the voltage-gated region and reaches the right (drain) side of the nanotrack. At the OFF state, both the microwave antenna and voltage gate are turned on. The microwave-excited SW drives the magnetic skyrmion moving toward the right, while the gate voltage, which results in the change of PMA in the voltage-gated region, leads to the stop of the magnetic skyrmion when it approaches the gate-induced potential barrier. The magnetic skyrmion cannot reach the drain side at the OFF state. The cones represent the magnetization, of which the out-of-plane component  $m_z$  is denoted by the orange-white-green color scale and the in-plane component  $m_x$  is denoted by the blue-gray-yellow color scale.

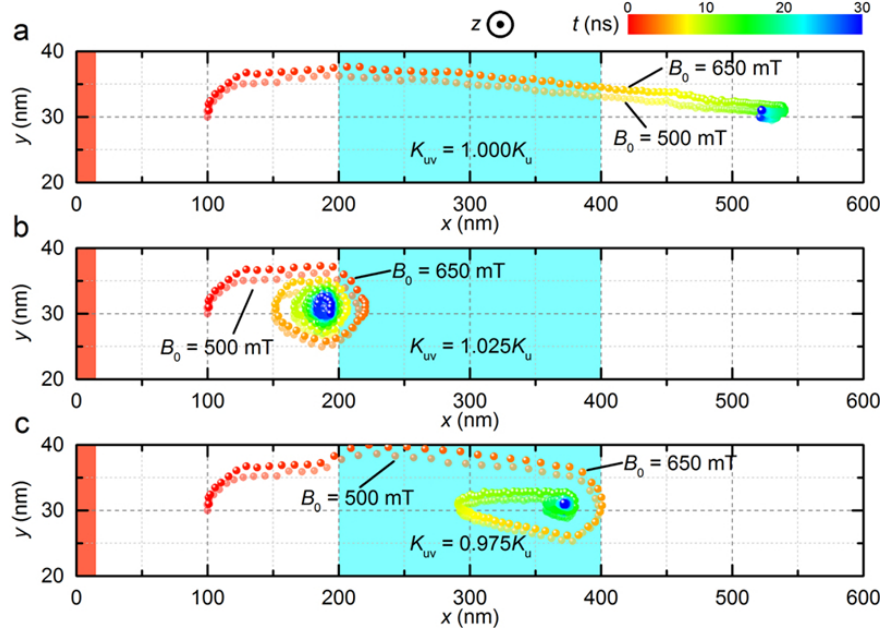


**Figure 2.** The trajectories of the magnetic skyrmion at the ON and OFF states driven by the microwave with different amplitudes. **(a)** The magnetic skyrmion transistor is in the ON state, where the microwave antenna is turned on and the voltage gate is turned off.  $B_0 = 500$  mT or 650 mT,  $f = 75$  GHz, similar hereinafter. The PMA in the voltage-gated region ( $K_{uv}$ ) equals that of the outside region ( $K_u$ ). **(b)** The magnetic skyrmion transistor is in the OFF state, where the microwave antenna and the voltage gate are turned on. The PMA in the voltage-gated region is larger than that of the outside region ( $K_{uv} = 1.025K_u$ ). **(c)** The magnetic skyrmion transistor is in the OFF state, where the microwave antenna and the voltage gate are turned on. The PMA in the voltage-gated region is smaller than that of the outside region ( $K_{uv} = 0.975K_u$ ). The dots denote the center of the magnetic skyrmion. The simulation time is 30 ns, which is indicated by the color scale. The red and blue regions stand for the regions where the microwave antenna and the voltage gate are deployed, respectively.

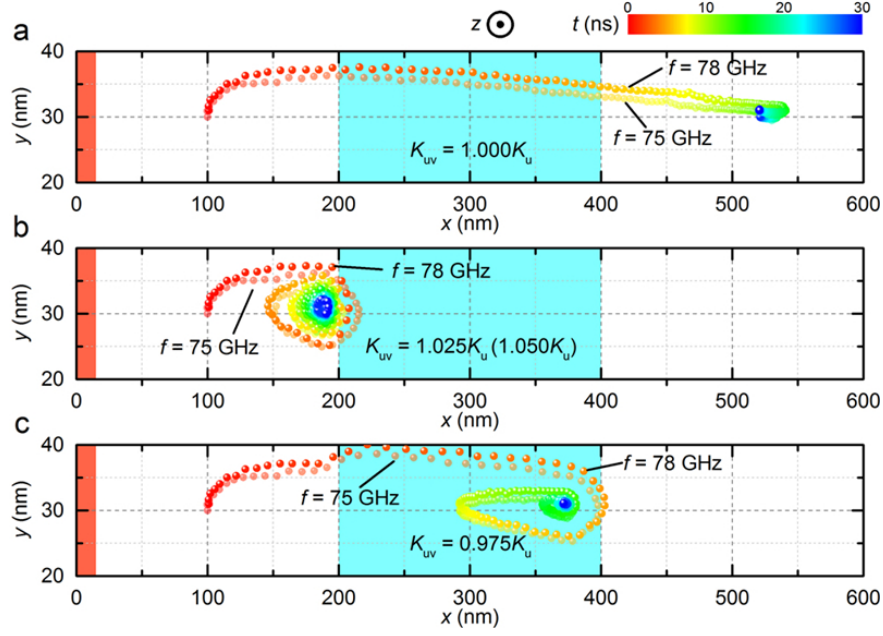


**Figure 3.** The trajectories of the magnetic skyrmion at the ON and OFF states driven by the microwave with different frequencies. (a) The magnetic skyrmion transistor is in the ON state, where the microwave antenna is turned on and the voltage gate is turned off.  $B_0 = 500$  mT,  $f = 75$  or  $78$  GHz, similar hereinafter. The PMA in the voltage-gated region ( $K_{uv}$ ) equals that of the outside region ( $K_u$ ). (b) The magnetic skyrmion transistor is in the OFF state, where the microwave antenna and the voltage gate are turned on. The PMA in the voltage-gated region is larger than that of the outside region (when  $f = 75$  GHz,  $K_{uv} = 1.025K_u$ , while when  $f = 78$  GHz,  $K_{uv} = 1.050K_u$ ). (c) The magnetic skyrmion transistor is in the OFF state, where the microwave antenna and the voltage gate are turned on. The PMA in the voltage-gated region is smaller than that of the outside region ( $K_{uv} = 0.975K_u$ ). The dots denote the center of the magnetic skyrmion. The simulation time is 30 ns, which is indicated by the color scale. The red and blue regions stand for the regions where the microwave antenna and the voltage gate are deployed, respectively.

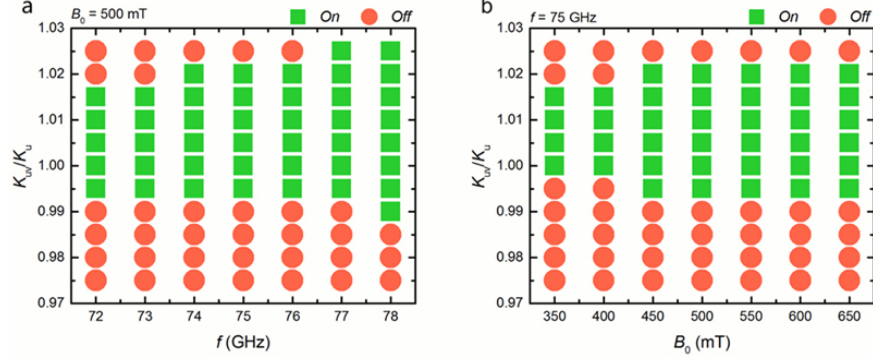


**Figure 4.** The working windows of the microwave-driven skyrmion transistor. **(a)** The working window at different gate voltages and microwave antenna excitation frequencies with a fixed microwave antenna excitation amplitude of 500 mT. **(b)** The working window at different gate voltages and microwave antenna excitation amplitudes with a fixed microwave antenna excitation frequency of 75 GHz. The square denotes the ON state, that is, the magnetic skyrmion passes the voltage-gated region moving from the source side to the drain side. The circle denotes the OFF state, that is, the magnetic skyrmion cannot pass the voltage-gated region and stops at the rest of the drain side.

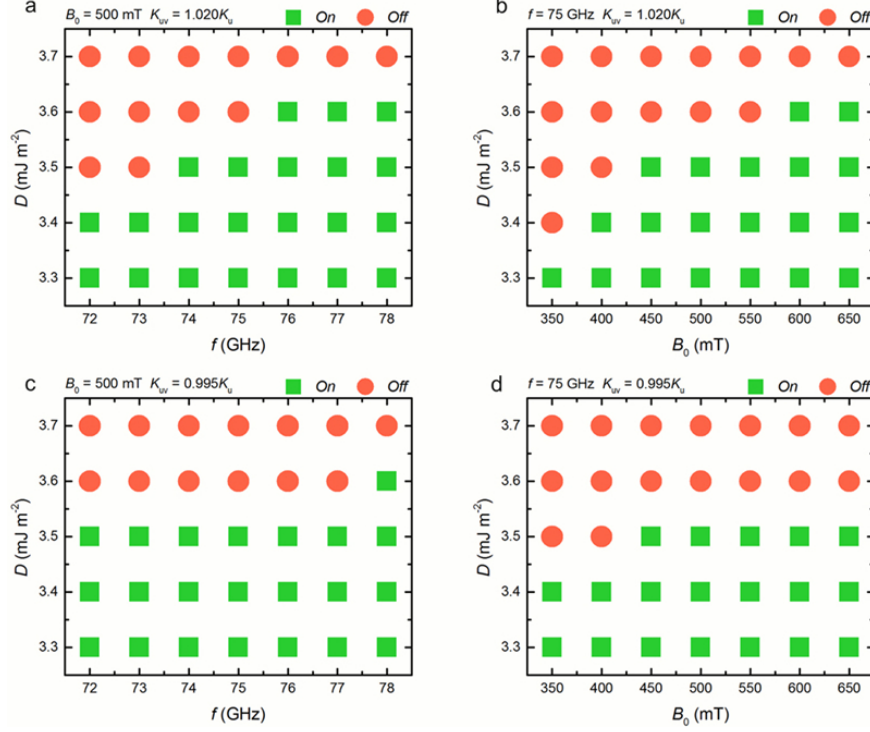


**Figure 5.** The effect of Dzyaloshinskii-Moriya interaction (DMI) on the working window of the microwave-driven skyrmion transistor. **(a)** The working window at different DMI and microwave antenna excitation frequencies with fixed  $K_{uv} = 1.020K_u$  and  $B_0 = 500$  mT. **(b)** The working window at different DMI and microwave antenna excitation amplitudes with fixed  $K_{uv} = 1.020K_u$  and  $f = 75$  GHz. **(c)** The working window at different DMI and microwave antenna excitation frequencies with fixed  $K_{uv} = 0.995K_u$  and  $B_0 = 500$  mT. **(d)** The working window at different DMI and microwave antenna excitation amplitudes with fixed  $K_{uv} = 0.995K_u$  and  $f = 75$  GHz. The square denotes the ON state, that is, the magnetic skyrmion passes the voltage-gated region moving from the source side to the drain side. The circle denotes the OFF state, that is, the magnetic skyrmion cannot pass the voltage-gated region and stops at the rest of the drain side.

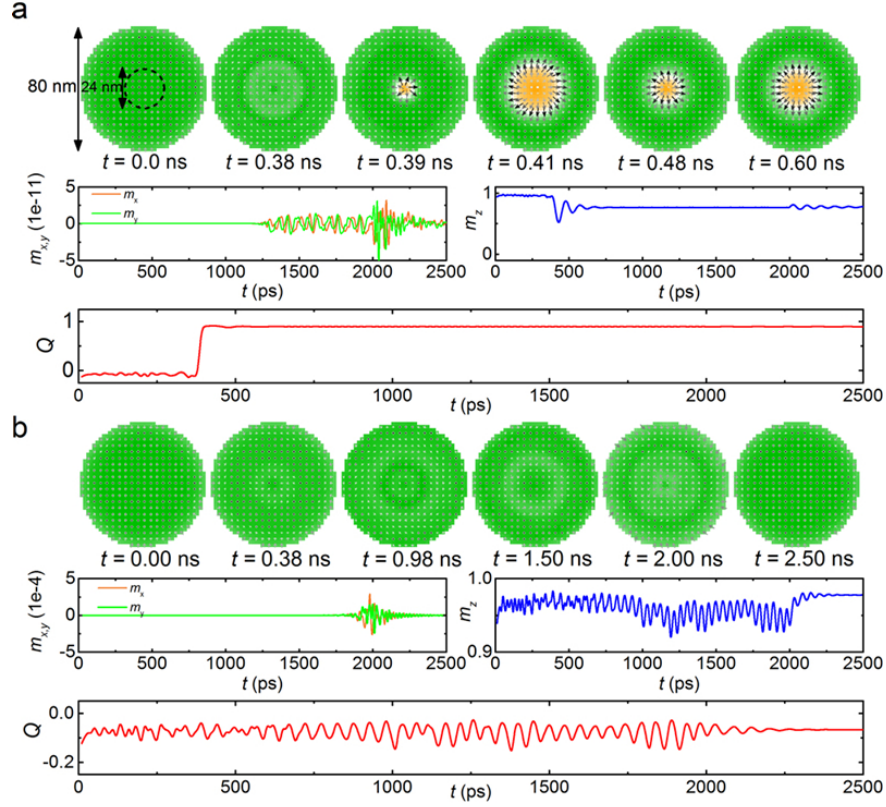


**Figure 6.** The microwave-current-assisted nucleation of the magnetic skyrmion. **(a)** Selected time evolution of the magnetization distribution, time-dependent  $m_x$ ,  $m_y$ ,  $m_z$ , and skyrmion number  $Q$  for the case of the skyrmion nucleation assisted by a microwave current with a selected frequency of  $f_{AC} = 53$  GHz. The diameter of the nanodisk equals 80 nm. The diameter of the current injection region equals 24 nm, which is denoted by the dashed circle in **(a)**. A spin-polarized DC current is applied in conjunction with an additional microwave current, that is,  $j_{\text{total}} = j_0 \sin 2\pi f_{AC} t + j_{DC}$ , to nucleate the magnetic skyrmion. Here,  $j_0 = 1 \times 10^{12} \text{ A m}^{-2}$  is the amplitude of the microwave current,  $j_{DC} = 1.8 \times 10^{12} \text{ A m}^{-2}$  is the current density of the DC current. A magnetic skyrmion can be nucleated successfully even  $j_{DC}$  is lower than the threshold current density,  $j_{th} = 2 \times 10^{12} \text{ A m}^{-2}$ . **(b)** Selected time evolution of the magnetization distribution, time-dependent  $m_x$ ,  $m_y$ ,  $m_z$ , and skyrmion number  $Q$  for the case of the skyrmion nucleation by applying only a DC spin current of  $j_{DC} = 1.8 \times 10^{12} \text{ A m}^{-2}$ . In the absence of the microwave current, the DC spin current itself of  $j_{DC} = 1.8 \times 10^{12} \text{ A m}^{-2}$  is unable to create the magnetic skyrmion. Only a subtle fluctuation of the skyrmion number  $Q$  is detected during the 2-ns-long current pulse, which is caused by the slight motion of the magnetization. The initial magnetization state of the nanodisk is along the  $+z$ -direction, and the polarization of the spin current is aligned along the  $-z$ -direction.



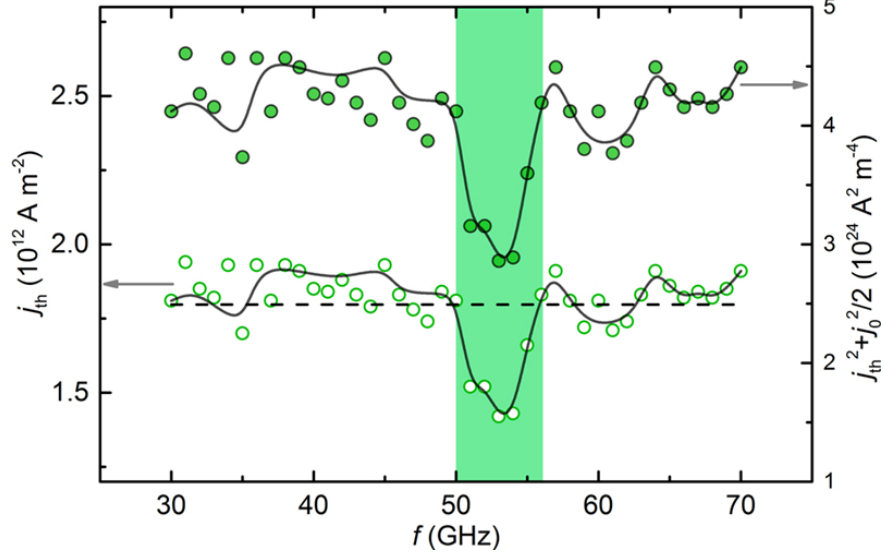


**Figure 7.** The effect of the frequency of the microwave current on the threshold current density required to create the magnetic skyrmion. The solid and open circles represent  $j_{\text{th}}^2 + j_0^2/2$  and the threshold current density  $j_{\text{th}}$  respectively. The amplitude  $j_0$  is fixed to be  $1.3 \times 10^{12} \text{ A m}^{-2}$ . The step of the frequency of microwave current is 1 GHz. The lines are guides to the eye. The assistance effect of the microwave current varies with its frequency  $f_{\text{AC}}$ , and the most effective frequency is indicated by green shadow. The dash line indicates the average value of the  $j_{\text{th}}$ .

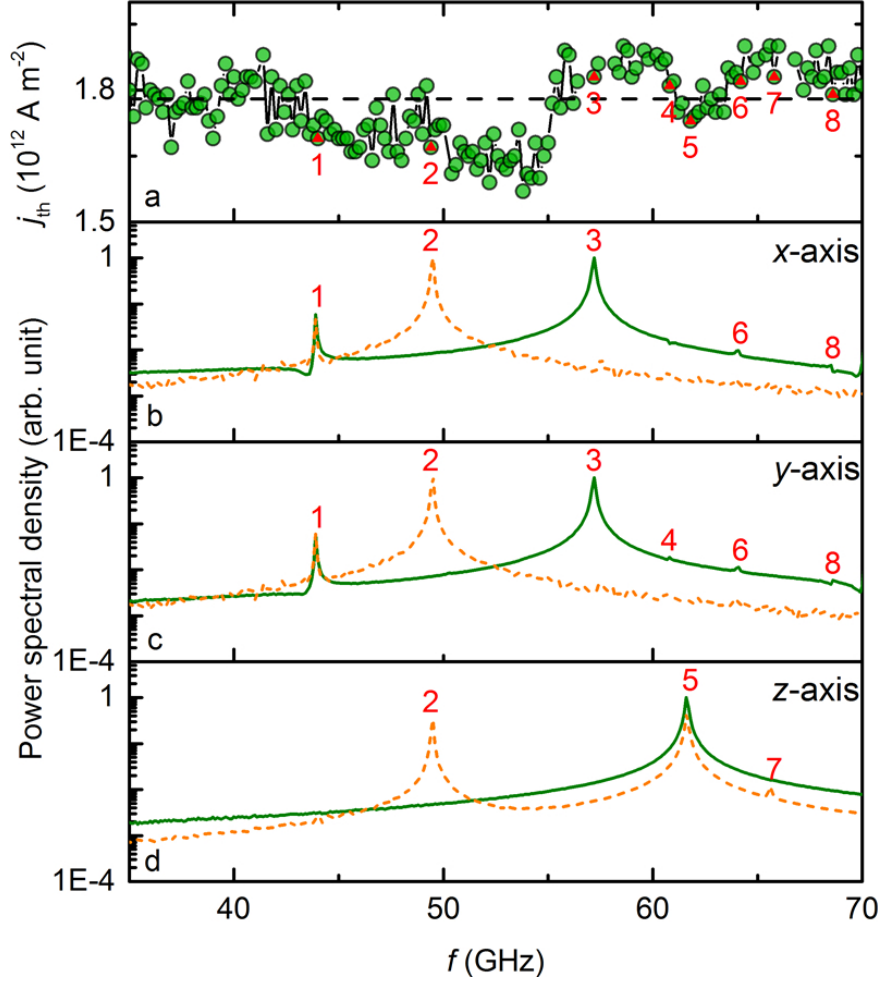


**Figure 8.** The threshold current density  $j_{th}$  as a function of the microwave current frequency  $f_{AC}$  with a fixed amplitude of  $j_0 = 1.0 \times 10^{12} \text{ A m}^{-2}$  and normalized power spectral densities. (a) The threshold current density  $j_{th}$  as a function of the microwave current frequency  $f_{AC}$ . The dash line indicates the average value of the  $j_{th}$ . (b) Spatially averaged (solid line) and spatially resolved (dash line) power spectral densities for  $x$ -axis excitation. (c) Spatially averaged (solid line) and spatially resolved (dash line) power spectral densities for  $y$ -axis excitation. (d) Spatially averaged (solid line) and spatially resolved (dash line) power spectral densities for  $z$ -axis excitation.

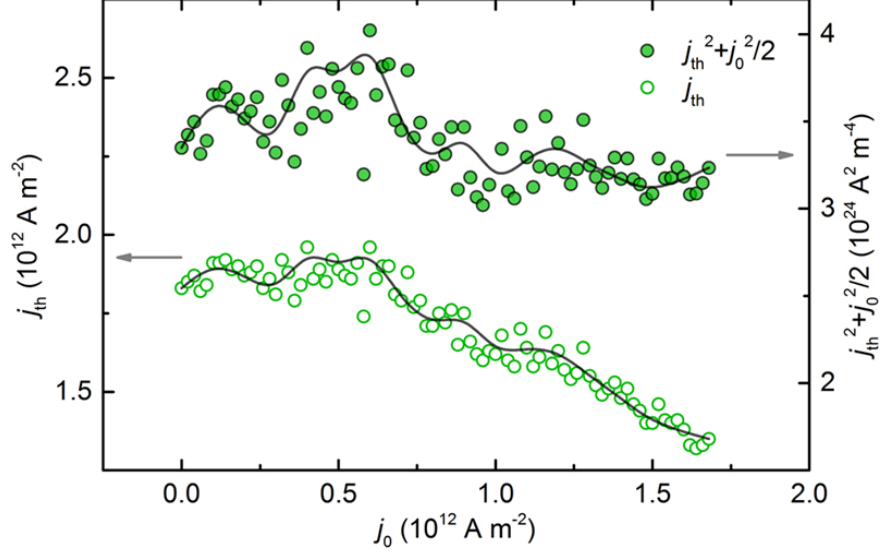


**Figure 9.** The effect of the amplitude of the microwave current on the threshold current required to create the magnetic skyrmion. The solid and open circles represent  $j_{\text{th}}^2 + j_0^2/2$  and the threshold current density  $j_{\text{th}}$  respectively. The microwave frequency  $f_{AC}$  is fixed to be 53 GHz. The step of the amplitude of microwave current is  $0.02 \times 10^{12} \text{ A m}^{-2}$ . The lines are guides to the eye.